Metrol. Meas. Syst., Vol. 28 (2021) No. 4, pp. 725–734
DOI: 10.24425/mms.2021.137708

PAN POLSKA AKADEMIA NAUK

METROLOGY AND MEASUREMENT SYSTEMS
Index 330930, ISSN 0860-8229
www.metrology.wat.edu.pl

M&MS

MAGNETOTRANSPORT MEASUREMENTS AS A TOOL FOR SEARCHING 3D TOPOLOGICAL INSULATORS

Paweł Śliż[1)], Iwona Sankowska[2)], Ewa Bobko[1)], Eugeniusz Szeregij[1)], Jakub Grendysa[1)], Grzegorz Tomaka[1)], Dariusz Żak[1)], Dariusz Płoch[1)], Agata Jasik[2)]

1) *University of Rzeszow, College of Natural Sciences, Institute of Physics, 1 Pigonia St., Rzeszow 35-959, Poland* (✉ *psliz@ur.edu.pl*, +48 178 518 678, *baranewa@ur.edu.pl, sheregii@ur.edu.pl, grendysa@ur.edu.pl, gmtomaka@o2.pl, 100gram@gazeta.pl, dploch@ur.edu.pl*)
2) *Łukasiewicz Research Network – Institute of Microelectronics and Photonics, al. Lotników 32/46, 02-668 Warsaw, Poland,* (*iwona.sankowska@imif.lukasiewicz.gov.pl, agata.jasik@imif.lukasiewicz.gov.pl*)

Abstract

The paper covers some measurement aspects of transport of electrons through metals and semiconductors in magnetic field – magnetotransport – allowing for the determination of electrical parameters characteristic of three-dimensional (3D) topological insulators (TI) (i.e. those that behave like an insulator inside their volume and have a conductive layer on their surface). A characteristic feature of the 3D TI is also a lack of differences between the chemical composition of the conductive surface and the interior of the material tested and the fact that the electron states for its surface conductivity are topologically protected. In particular, the methods of generating strong magnetic fields, obtaining low temperatures, creating electrical contacts with appropriate geometry were presented, and the measurement methods were reviewed. In addition, the results of magnetotransport measurements obtained for two volumetric samples based on the HgCdTe compound grown with the molecular beam epitaxy method are presented.

Keywords: materials science, magnetotransport, topological insulators, quantum Hall effect.

1. Introduction

The three-dimensional (3D) *topological insulator* (TI) is a new state of matter in which material behaves like an insulator inside its volume and has a conductive layer on its surface. Two characteristic features of a 3D TI are a lack of differences between the chemical composition of the conductive surface and the interior of the material, and the fact that the electron states responsible for its surface conductivity are topologically protected (TPSS) by time-reversal symmetry. These states are resistant to disturbances caused by *e.g.* impurities. The theoretical description of the nature of 3D TI was introduced in 2007 [1] and experimentally confirmed in $Bi_{1-x}Sb_x$ in 2008 [2] by *angle-resolved photoemission spectroscopy* (ARPES). *Magnetotransport* (MT) is another tool

Article history: received June 25, 2021; revised August 6, 2021; accepted August 13, 2021; available online August 31, 2021.

used to confirm the existence of TPSS. It allows for electrical characterization of 3D TI over a wide range of temperatures and magnetic fields [3–7]. In contrast to ARPES, MT can identify the topological phase in more complex structures in which material surface is optically unavailable, *e.g.* in a HgTe quantum well with barriers [8], [9]. In this method, a 2D electronic transport in a high magnetic field perpendicular to the surface is manifested by the *integer quantum Hall effect* (IQHE) [10–13]. *Shubnikov-de Haas* (SdH) oscillations are analyzed to confirm the presence of TPSS. It allows identification of the Berry phase value equal to π, which corresponds to 1/2 intersection for a linear fit of the N-th SdH minima as a function of *1/B* [14, 15]. On the other hand, the MT technique records the total conductivity. In the case when the bulk of the sample behaves like a semiconductor or a semi-metal the contribution of surface and bulk conductivity to the total conductivity can be difficult to determine [16]. The article strengthens the efforts of the cited and other research groups [12] in the development of the MT technique as a useful tool for the study of subtle physical phenomena occurring in mature materials or their heterostructures including the identification of TI features in 3D HgCdTe heterostructures. In-depth knowledge and description of these phenomena will allow for their practical application in the future, *e.g.* in spintronics and quantum computing. In the first sections, aspects of the MT and the results obtained using this method, next the results obtained with other methods confirming the MT performance are presented.

2. Magnetotransport – technical aspects of the measurement system

The key technical aspects of the magnetotransport method refer to a high magnetic field, low temperature [17, 18], and acquiring electrical signals for resistance measurement [19]. For generating a magnetic field of up to 41 T, the DC resistive magnets can be used [20]. Their disadvantage is a high power requirement in the megawatt range. Superconducting magnets do not have this drawback, but they generate magnetic fields only up to 32 T [21]. The combination of DC and superconducting magnets allows one to generate a magnetic field up to 45 T [6, 22]. Higher fields can only be obtained using impulse methods [23, 24]. To eliminate the thermal effects masking quantum phenomena, low-temperature cooling must be used. For temperatures 1.2–4.2 K and higher, liquid ^{4}He is used and for temperatures > 0.4 K an additional system filled with ^{3}He is necessary. Measurement of temperature in the range of 0.3–420 K in a magnetic field can be carried out *e.g.* with ZrO_xN_y thin-film thermistors [25, 26] or RuO_2 thermometers [27]. To acquire electrical signals for resistance measurements, the *DC* method uses a precise DC source and voltmeters. The *Lock-in* method uses AC forcing and the measured signals are detected by the phase-sensitive amplifier. This method eliminates the influence of interfering signals in frequencies and phases different than the forcing signal [28, 29]. A method called the *Delta mode* using a precise nano-voltmeter controlled by AC source largely eliminates the influence of low-frequency disturbance, *e.g.* DC offset or thermoelectric voltages [30–32].

The magnetotransport experimental setup presented in Fig. 1 uses an ICEoxford cryostat with a superconducting magnet capable of generating magnetic fields up to 14 T powered by an AMI 4Q06125PS power supply with an AMI 430 controller. For resistance measurement, the four-point and the constant-current method with a successive change of its direction were used with a KEITHLEY 2634B current source (with typical sample excitation current of 1 μA or 5 μA) and three KEITHLEY 2002 8.5-digit resolution multimeters (two for the V_{xx} voltages and another one for the V_{xy} voltage measurements). The MT measurements controlled with a Lake Shore 336 precision four-channel PID temperature controller were performed over a wide temperature range from 1.2 K to 60 K. To obtain the necessary thermal insulation between the sample and

Metrol. Meas. Syst., Vol. 28 (2021), No. 4, pp. 725–734
DOI: 10.24425/mms.2021.137708

the liquid helium bath, vacuum was created (before cooling the sample holder) by means of a Pfeiffer HiCube 80 Eco turbo molecular vacuum pump. In order to obtain sample temperature below 4.2 K, helium vapor pressure in the helium pot (located near the sample) was reduced with a SOGEVAC SV40B rotary vane pump with pressure measuring using an INFICON PGD400 Pirani gauge controller and a PSG500 Pirani gauge. Analog signal from the PGD400 was acquired and converted to digital data with a UNI-T UT803 multimeter. The level of liquid helium in the cryostat was recorded with a TSI HDI-AI helium depth indicator with a superconducting helium level probe. A PC computer with interfaces GPIB, LAN, USB, RS232C and with LabVIEW software [33] was used for the control, acquisition and visualization of measurement data in real time. This system allowed for the determination of electrical parameters of 2D electron gas and identification of IQHE and SdH oscillations.

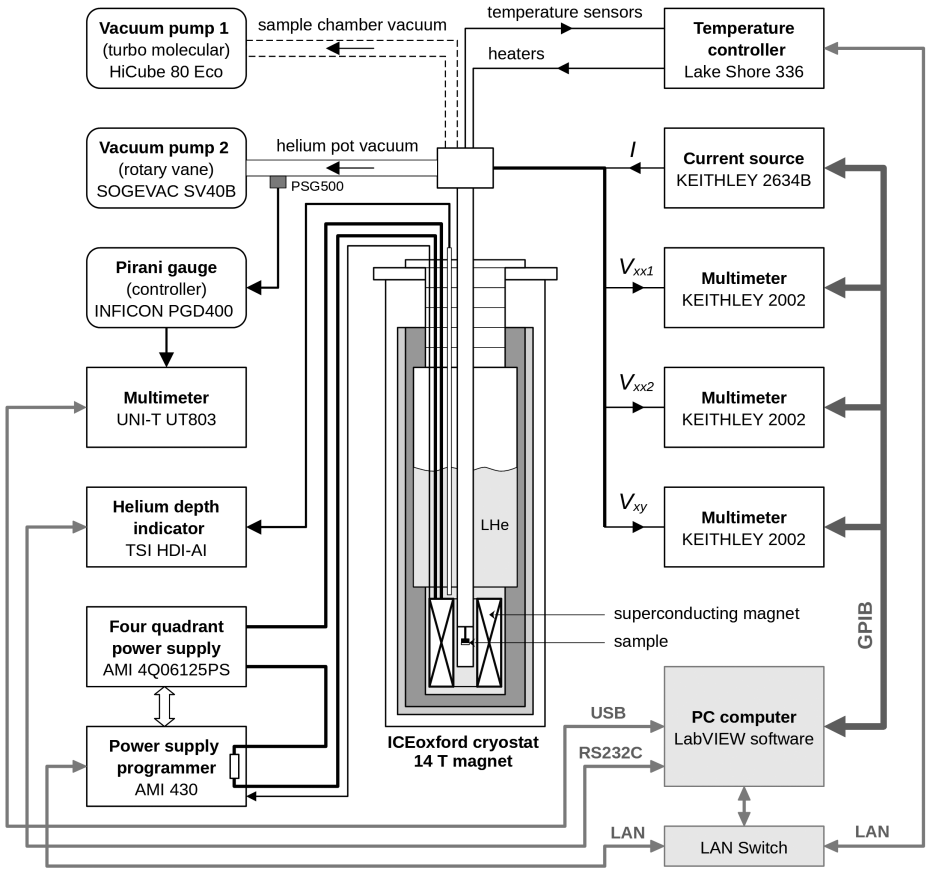

Fig. 1. Diagram of the measurement system used for the magnetotransport experiment.

3. Sample preparation

Two different samples of HgCdTe were chosen to demonstrate the usefulness of MT in 3D TI identification. They were grown using a MBE Ribber Compact 21 reactor. For sample S1, a ZnTe wetting layer (of several nm) was deposited on a GaAs (001) substrate followed by

a CdTe buffer ($d_{\mathrm{CdTe}} > 1.2$ μm) and an iodine doped $Hg_{1-x}Cd_xTe$ layer. For sample S2, an indium doped $Hg_{1-x}Cd_xTe$ layer was grown directly on a CdZnTe (211) substrate. The chemical composition and thickness of $Hg_{1-x}Cd_xTe$ layers were estimated using the *high-resolution X-ray diffraction* (HRXRD) method. The electrical contacts for sample S1 were made by direct soldering ($T = 180$°C) of indium onto its surface in a Hall bar geometry (without lithography). For sample S2, the electron-beam lithography was used to make six contacts in the Hall bar geometry with a 100 μm current channel width and 240 μm longitudinal contacts separation. The samples were connected to the holder of the measurement system using gold wires 80 μm in diameter.

4. Electrical characterization employing the magnetotransport

The R_{xx} and R_{xy} measurement data as a function of magnetic field B in the temperature range of 1.2–50 K for sample S1 and 1.27–60 K for sample S2 were collected and are shown in Fig. 2. The SdH oscillations for R_{xx} and IQHE for R_{xy} were visible over a wide range of temperatures.

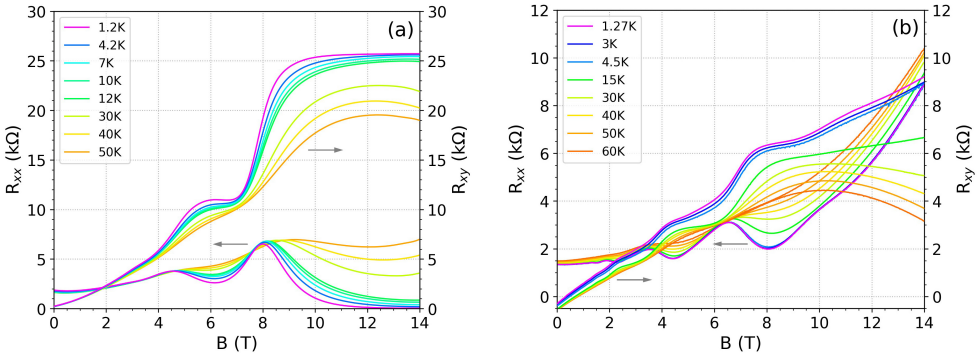

Fig. 2. R_{xx} and R_{xy} versus magnetic field B at various temperatures obtained for (a) sample S1 and (b) sample S2.

To confirm the presence of TPSS in the investigated samples, the positions of minima and maxima of SdH oscillations were identified in the ΔR_{xx} data (obtained by quadratic function background subtraction from R_{xx}) in $1/B$ inverse magnetic field, which are presented in Fig. 3. The intercept point b of the linear fit of N-th SdH oscillation (integer values for SdH minima and half values for SdH maxima) in $1/B$ for identification of the Berry phase and the TPSS are shown in the inserts. The results obtained were 0.609 and 0.887 for samples S1 and S2, respectively. The value for the first sample is close to the theoretical value of 1/2 specific for TI [15], whereas the result for the second one is closer to 1 and indicates the absence of TPSS.

The mobility μ and sheet carrier concentration n_s were calculated from slope R_{xy} at $B = 1$ T and R_{xx0} data for $B = 0$ T. Sheet carrier concentration $n_s = nd$, where n is carrier concentration and d is sample thickness. The carrier concentration derived from the Hall effect is $n = 1/(R_H e)$, where e is charge of carrier and R_H is Hall coefficient obtained from the MT experiment: $R_H = (R_{xy}/B)d$, where $R_{xy} = R_{xy}|_{(B=1\,\mathrm{T})} - R_{xy}|_{(B=0\,\mathrm{T})}$ and B is magnetic field. The final formula for sheet carrier concentration is:

$$n_s = \frac{B}{eR_{xy}}\,. \tag{1}$$

The mobility obtained from the Hall effect is equal to $\mu = \sigma R_H$, where σ is conductivity calculated from longitudinal resistance R_{xx0} at magnetic field B = 0 T and equal to $\sigma = l/(R_{xx0}wd)$,

Metrol. Meas. Syst., Vol. 28 (2021), No. 4, pp. 725–734
DOI: 10.24425/mms.2021.137708

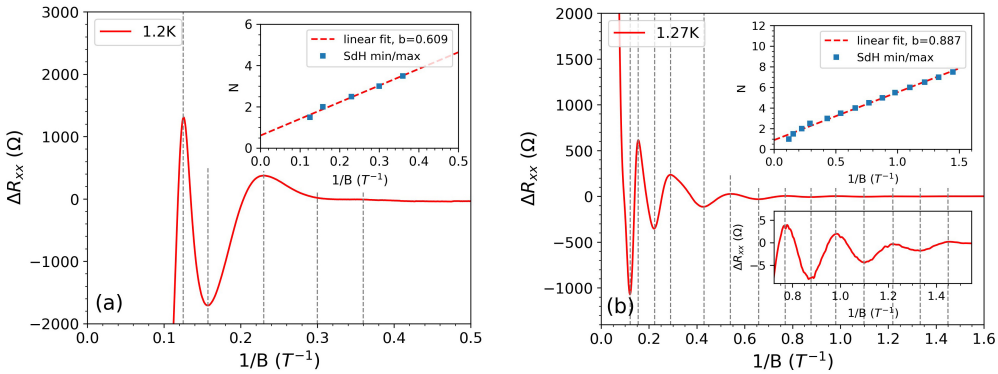

Fig. 3. ΔR_{xx} as a function of inverse magnetic field $1/B$ for (a) sample S1 at 1.2 K, (b) sample S2 at 1.27 K. Inserts – squares: position of N-th SdH maxima and minima, dotted line: best linear fit for N-th SdH minima/maxima as a function of $1/B$.

where w is sample current channel width and l is longitudinal R_{xx} contacts separation. The final equation for mobility calculation is:

$$\mu = \frac{R_{xy}}{R_{xx0}} \frac{l}{wB} \,. \tag{2}$$

The electrical parameters obtained from (1) and (2) for the investigated HgCdTe samples at temperatures of 1.2 (1.27) K and 50 K are presented in Table 1.

Table 1. Sheet carrier concentration and mobility for investigated HgCdTe samples S1 and S2.

Temperature	1.2 (1.27) [K]		50 [K]	
Sample	n_s [1/cm^2]	μ [cm^2/(V·s)]	n_s [1/cm^2]	μ [cm^2/(V·s)]
S1	7.60×10^{11}	3674	7.74×10^{11}	3950
S2	7.46×10^{11}	14954	8.68×10^{11}	11903

Sheet carrier concentration was similar for both samples, while the mobility measured at low (high) temperature for sample S2 was about four (three) times larger than that for sample S1.

5. Structural characterization employing the AFM and HR XRD methods

A Solver Nano NT-MDT *atomic force microscope* (AFM) was used for surface characterization of the investigated samples. The AFM topography of 10×10 μm areas is shown in Fig. 4. The obtained RMS roughness (after subtracting the background with a 5th-order polynomial) was 5.76 nm and 1.78 nm for samples S1 and S2, respectively.

The structural investigations were carried out using the HRXRD technique. Symmetrical $2\theta/\omega$ scans and reciprocal space maps around 004 and 115 GaAs(100) *reciprocal lattice points* (RLP) for sample S1 and 422, 333, 511, 440, and 404 (for different azimuths) $Cd_yZn_{(1-y)}Te(211)$ RLP for sample S2 were measured. The HRXRD mapping for sample S1 showed that the CdTe buffer layer was relaxed (Fig. 5b) and the elongation of CdTe RLP in Q_x and Q_z caused by misfit dislocations

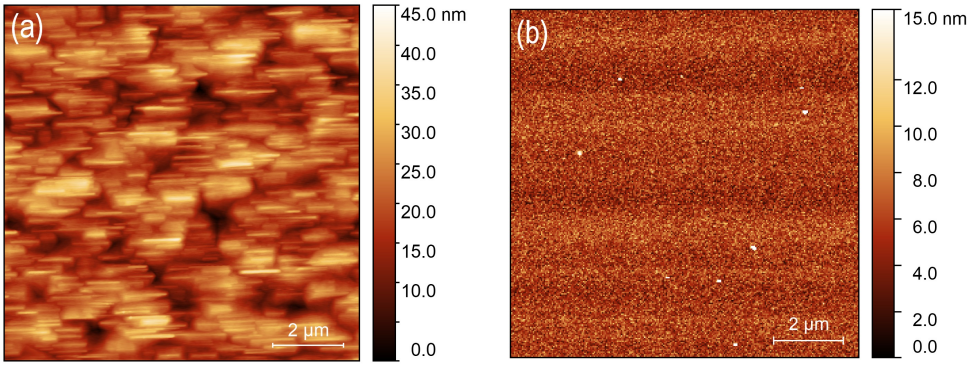

Fig. 4. AFM topography of 10 × 10 μm surface area of (a) sample S1, (b) sample S2.

was observed (Fig. 5a). Furthermore, the intensity of $Hg_{(1-x)}Cd_xTe$ RLP was very small, the ZnTe layer was not detected. As the crystal quality of sample S1 was poor, the lattice constants (perpendicular (⊥) and parallel (||)) and stoichiometric coefficient x in $Hg_{(1-x)}Cd_xTe$ layer were difficult to determine precisely. The layer thickness seems to be closer to 50 nm than to the value of 100 nm assumed for MBE growth. The diffraction measurements of sample S2 revealed a

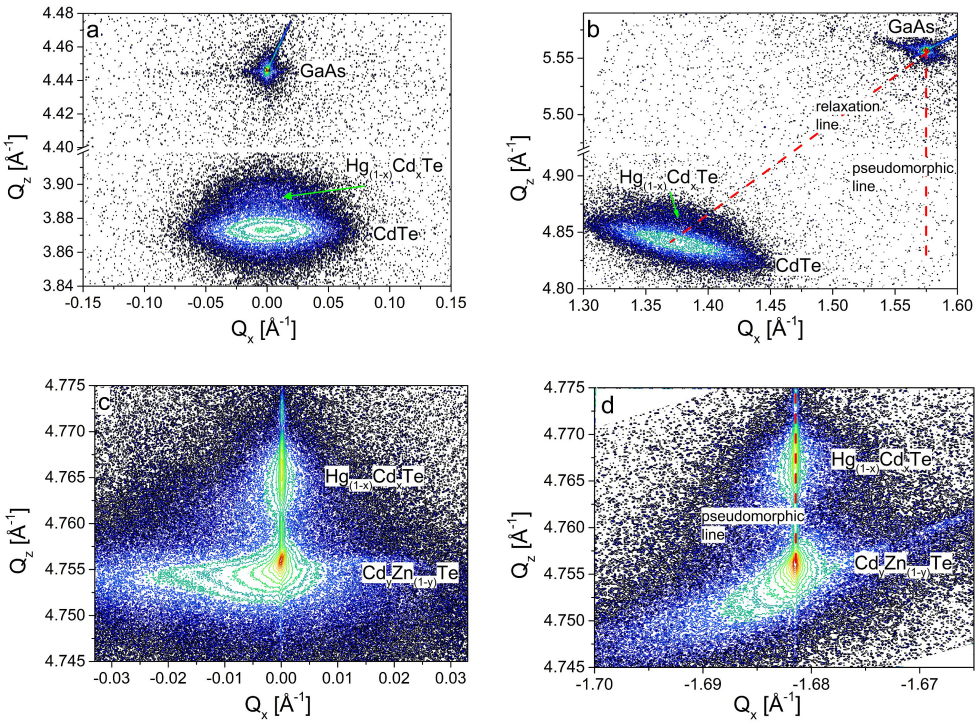

Fig. 5. The reciprocal space maps around symmetrical 004 (a) and asymmetrical (115) (b) GaAs reciprocal lattice points for sample S1 and symmetrical 442 (c) and asymmetrical (333) (d) $Cd_yZn_{(1-y)}Te$ ones for sample S2. The pseudomorphic and relaxation lines indicate the relaxation of 0% and 100%, respectively.

Metrol. Meas. Syst., Vol. 28 (2021), No. 4, pp. 725–734
DOI: 10.24425/mms.2021.137708

pseudomorphic growth of the $Hg_{(1-x)}Cd_xTe$ layer on the $Cd_yZn_{(1-y)}Te$ substrate (Fig. 5d). The layer was well defined and thickness fringes were observed so the lattice constants and composition were precisely determined. Diffuse scattering observed around the $Cd_yZn_{(1-y)}Te$ RLP indicates a large number of defects present in the substrate. The analysis of sample S2 was performed based on the approach described in [34]. The quantitative results of HRXRD analysis of sample S1 were as follows: $a_{(GaAs)} = 5.65291$ Å, $a_{\perp(CdTe)} = 6.48889$ Å, $a_{\parallel(CdTe)} = 6.46950$ Å, the relaxation of the CdTe buffer was R = 99.2%, $(\Delta a/a)_{\perp}$ CdTe to GaAs = 15×10^4 ppm, $a_{\perp(Hg_{(1-x)}Cd_xTe)} \approx 6.45557$ Å, $a_{\parallel(Hg_{(1-x)}Cd_xTe)} \approx 6.46950$ Å, $x = 0.16$ in $Hg_{(1-x)}Cd_xTe$, $Hg_{(1-x)}Cd_xTe$ thickness ~ 50 nm, the relaxation of $Hg_{(1-x)}Cd_xTe$ was R = 0%, $(\Delta a/a)_{\perp}$ of $Hg_{(1-x)}Cd_xTe$ to CdTe = −5100 ppm. The parameters for sample S2 were: $a_{(Cd_yZn_{(1-y)}Te_{substrate})} = 6.47212$ Å, $a_{\perp(Hg_{(1-x)}Cd_xTe)} \sim 6.45861$ Å, $a_{\parallel(Hg_{(1-x)}Cd_xTe)} \approx 6.47183$ Å, $x = 0.185$ in $Hg_{(1-x)}Cd_xTe$, $Hg_{(1-x)}Cd_xTe$ thickness ≈ 146 nm, the relaxation of $Hg_{(1-x)}Cd_xTe$ was R = 4%, $(\Delta a/a)\perp Hg_{(1-x)}Cd_xTe$ to $Cd_yZn_{(1-y)}Te$ = −2090 ppm.

6. Analysis of results

The MT data obtained indicate that sample S1 is 3D TI and sample S2 does not fulfill the criteria for the 3D TI. The intercept point b of the linear fit of N-th SdH oscillation in $1/B$ were 0.609 and 0.887 for sample S1 and S2, respectively. This analysis of the obtained MT results was confirmed by with both HRXRD and AFM. The X-ray diffraction data shows that the HgCdTe layer was fully strained (R = 0%) but of poor structural quality. The stoichiometric coefficient $x \sim 0.16$ corresponds to $E_g < 0$ eV at LHe temperature. Sample S2 was partially relaxed (R = 4%) with $x = 0.185$, which corresponds to $E_g > 0$ eV. This means that no band structure conversion occurs on the lower and upper interfaces and therefore there are no TPSS. MT data for sample S1 indicate relatively low mobility caused by carrier scattering on one or both geometrically rough interfaces. Sample S2 had lower surface roughness measured using AFM than sample S1, which justifies the higher mobility of the former. The obtained results proved that MT is a sufficient technique to uniquely identify TI features in complex HgCdTe heterostructures.

7. Conclusions

The described MT method and the measurement system applied have proved suitable to recognize the electrical properties characteristic for 3D TI by analyzing both IQHE and SdH oscillations. The presented MT data obtained for two HgCdTe samples demonstrated the cases with presence and lack of 3D TI features. Ancillary methods (AFM, HRXRD) used for characterization of both surface and crystal structure of the measured samples confirmed the usefulness and importance of MT results in the field of 3D TI characterization.

References

[1] Fu, L., Kane, C. L., & Mele, E. J. (2007). Topological Insulators in Three Dimensions. *Physical Review Letters*, *98*(10), 106803. https://doi.org/10.1103/physrevlett.98.106803

[2] Hsieh, D., Qian, D., Wray, L., Xia, Y., Hor, Y. S., Cava, R. J., & Hasan, M. Z. (2008). A topological Dirac insulator in a quantum spin Hall phase. *Nature*, *452*(7190), 970–974. https://doi.org/10.1038/nature06843

[3] Xu, Y., Miotkowski, I., Liu, C., Tian, J., Nam, H., Alidoust, N., Hu, J., Shih, C.-K., Hasan, M. Z., & Chen, Y. P. (2014). Observation of topological surface state quantum Hall effect in an intrinsic three-dimensional topological insulator. *Nature Physics*, *10*(12), 956–963. https://doi.org/10.1038/nphys3140

[4] Qu, D.-X., Hor, Y. S., Xiong, J., Cava, R. J., & Ong, N. P. (2010). Quantum Oscillations and Hall Anomaly of Surface States in the Topological Insulator Bi_2Te_3. *Science*, *329*(5993), 821–824. https://doi.org/10.1126/science.1189792

[5] Analytis, J. G., McDonald, R. D., Riggs, S. C., Chu, J.-H., Boebinger, G. S., & Fisher, I. R. (2010). Two-dimensional surface state in the quantum limit of a topological insulator. *Nature Physics*, *6*(12), 960–964. https://doi.org/10.1038/nphys1861

[6] Shrestha, K. (2015). *Magnetotransport Studies on Topological Insulators* [Doctoral dissertation, University of Houston]. https://uh-ir.tdl.org/handle/10657/4881

[7] Zhang, J. (2016). *Transport Studies of the Electrical, Magnetic and Thermoelectric Properties of Topological Insulator Thin Films*. Springer-Verlag GmbH

[8] König, M., Wiedmann, S., Brüne, C., Roth, A., Buhmann, H., Molenkamp, L. W., Qi, X.-L., & Zhang, S.-C. (2007). Quantum Spin Hall Insulator State in HgTe Quantum Wells. *Science*, *318*(5851), 766–770. https://doi.org/10.1126/science.1148047

[9] Shamim, S., Beugeling, W., Böttcher, J., Shekhar, P., Budewitz, A., Leubner, P., Lunczer, L., Hankiewicz, E. M., Buhmann, H., & Molenkamp, L. W. (2020). Emergent quantum Hall effects below 50 mT in a two-dimensional topological insulator. *Science Advances*, *6*(26). https://doi.org/10.1126/sciadv.aba4625

[10] Weis, J., & von Klitzing, K. (2011). Metrology and microscopic picture of the integer quantum Hall effect. *Philosophical Transactions of the Royal Society A: Mathematical, Physical and Engineering Sciences*, *369*(1953), 3954–3974. https://doi.org/10.1098/rsta.2011.0198

[11] K. I. Wysokiński. (2006). Quantum Hall effect: the fundamentals. *Metrology and Measurement Systems*, *13*(2), 113–124. http://www.metrology.pg.gda.pl/full/2006/M&MS_2006_113.pdf

[12] Brüne, C., Liu, C. X., Novik, E. G., Hankiewicz, E. M., Buhmann, H., Chen, Y. L., Qi, X. L., Shen, Z. X., Zhang, S. C., & Molenkamp, L. W. (2011). Quantum Hall effect from the topological surface states of strained bulk HgTe. *Physical Review Letters*, *106*(12), 126803. https://doi.org/10.1103/PhysRevLett.106.126803

[13] Brüne, C., Thienel, C., Stuiber, M., Böttcher, J., Buhmann, H., Novik, E. G., Liu, C.-X., Hankiewicz, E. M., & Molenkamp, L. W. (2014). Dirac-Screening Stabilized Surface-State Transport in a Topological Insulator. *Physical Review X*, *4*(4), 41045. https://doi.org/10.1103/PhysRevX.4.041045

[14] Mikitik, G. P., & Sharlai, Y. V. (1999). Manifestation of Berry's Phase in Metal Physics. *Physical Review Letters*, *82*(10), 2147–2150. https://doi.org/10.1103/physrevlett.82.2147

[15] Taskin, A. A., & Ando, Y. (2011). Berry phase of nonideal Dirac fermions in topological insulators. *Physical Review B*, *84*(3), 35301. https://doi.org/10.1103/physrevb.84.035301

[16] Tomaka, G., Grendysa, J., Śliż, P., Becker, C. R., Polit, J., Wojnarowska, R., Stadler, A., & Sheregii, E. M. (2016). High-temperature stability of electron transport in semiconductors with strong spin-orbital interaction. *Physical Review B*, *93*(20), 205419. https://doi.org/10.1103/physrevb.93.205419

[17] Melhem, Z. (2019). *Cryogenics at Oxford Instruments*. Oxford Instruments. https://indico.cern.ch/event/792215/contributions/3408669/attachments/1938018/3212326/Melhem_Ziad_Cryo_at_OI_EasiTrain_2Oct19_.pdf

[18] Balshaw, N. H. (1996). *Practical Cryogenics: An Introduction to Laboratory Cryogenics*. Oxford Instruments, Scientific Research Division

Metrol. Meas. Syst., Vol. 28 (2021), No. 4, pp. 725–734
DOI: 10.24425/mms.2021.137708

[19] LakeShore. (n.d.). *Lake Shore 7500/9500 Series Hall System User's Manual*. http://sites.science.oregonstate.edu/~tatej/TateLabWiki/lib/exe/fetch.php?media=manuals:lakeshore_7504_complete.pdf

[20] MagLab. (2018). *National MagLab – Elevate your research with higher fields. Brochure*. https://nationalmaglab.org/images/research/publications/searchable_docs/print_media/maglab_elevate_brochure_2018.pdf

[21] Markiewicz, W. D., Larbalestier, D. C., Weijers, H. W., Voran, A. J., Pickard, K. W., Sheppard, W. R., Jaroszynski, J., Xu, A., Walsh, R. P., Lu, J., Gavrilin, A. V, & Noyes, P. D. (2012). Design of a Superconducting 32 T Magnet With REBCO High Field Coils. *IEEE Transactions on Applied Superconductivity*, *22*(3), 4300704. https://doi.org/10.1109/tasc.2011.2174952

[22] Hahn, S., Kim, K., Kim, K., Hu, X., Painter, T., Dixon, I., Kim, S., Bhattarai, K. R., Noguchi, S., Jaroszynski, J., & Larbalestier, D. C. (2019). 45.5-tesla direct-current magnetic field generated with a high-temperature superconducting magnet. *Nature*, *570*(7762), 496–499. https://doi.org/10.1038/s41586-019-1293-1

[23] Nakamura, D., Ikeda, A., Sawabe, H., Matsuda, Y. H., & Takeyama, S. (2018). Record indoor magnetic field of 1200 T generated by electromagnetic flux-compression. *Review of Scientific Instruments*, *89*(9), 95106. https://doi.org/10.1063/1.5044557

[24] Liu, Q., Zhang, S., Ding, L., Zuo, H., & Han, X. (2019). Magnetoresistance Measurement of Topological Quantum Materials in Pulsed High Magnetic Field. *2019 IEEE International Instrumentation and Measurement Technology Conference (I2MTC)*, 1–6. https://doi.org/10.1109/I2MTC.2019.8827073

[25] Courts, S. S. (2003). Review of Cernox^{TM} (Zirconium Oxy-Nitride) Thin-Film Resistance Temperature Sensors. *AIP Conference Proceedings*, *684*, 393–398. https://doi.org/10.1063/1.1627157

[26] Kowalewski, A., Wróbel, J., Boguski, J., Gorczyca, K., & Martyniuk, P. (2019). Semiconductor contact layer characterization in a context of hall effect measurements. *Metrology and Measurement Systems*, *26*(1), 109–114. https://doi.org/10.24425/mms.2019.126324

[27] Mleczko, K., & Ptak, P. (2015). Low-temperature properties of RuO_2-based resistors. *Scientific Journals of Rzeszów University of Technology, Series: Electrotechnics*, 275–294. https://doi.org/10.7862/re.2015.21

[28] ZurichInstruments. (n.d.). *Hall Effect for Sensing and Materials Characterization*. https://www.zhinst.com/europe/en/publications/hall-effect-sensing-and-materials-characterization

[29] Vaklinova, K. (2017). *Spin Transport in Topological Insulator-Based Nanostructures,* [Doctoral dissertation, École Polytechnique Fédérale de Lausanne]. https://doi.org/10.5075/epfl-thesis-7585

[30] Chiatti, O., Riha, C., Lawrenz, D., Busch, M., Dusari, S., Sánchez-Barriga, J., Mogilatenko, A., Yashina, L. V, Valencia, S., Ünal, A. A., Rader, O., & Fischer, S. F. (2016). 2D layered transport properties from topological insulator Bi_2Se_3 single crystals and micro flakes. *Scientific Reports*, *6*(1). https://doi.org/10.1038/srep27483

[31] Meyyappa, M. (2007). *Nanotechnology Measurement Handbook. A Guide to Electrical Measurements for Nanoscience Applications*. Keithley Instruments, Inc. https://download.tek.com/document/1KW-30011-0%20NanotechHandbook.pdf

[32] Suslov, A. V. (2010). Stand alone experimental setup for dc transport measurements. *Review of Scientific Instruments*, *81*(7), 75111. https://doi.org/10.1063/1.3463691

[33] Nawrocki, W. (2005). *Measurement Systems and Sensors*. Artech House

[34] Sewell, R. H., Musca, C. A., Dell, J. M., Faraone, L., Usher, B. F., & Dieing, T. (2005). High-resolution X-ray diffraction studies of molecular beam epitaxy-grown HgCdTe heterostructures and CdZnTe substrates. *Journal of Electronic Materials*, *34*(6), 795–803. https://doi.org/10.1007/s11664-005-0023-7

Paweł Śliż obtained the M.Sc. degree in Physics from the University of Rzeszow, Poland, in 2002. From that year to 2008 he was employed as a senior technical clerk at the Institute of Physics, University of Rzeszow. From 2015 he has been assistant at the Centre for Microelectronics and Nanotechnology, University of Rzeszow. His research activity focuses on magnetotransport measurements in high magnetic fields and low temperatures of II-VI and III-V structures and analyzing measurement data in Python and LabVIEW environment.

Iwona Sankowska received the Ph.D. degree from the Faculty of Physics, University of Warsaw, Poland, in 2008. She is currently Senior Research Specialist with the Department of Photonics, Łukasiewicz Research Network – Institute of Microelectronics and Photonics, Warsaw. She specializes in crystal characterization of semiconductor periodic structures (e.g. type II InAs/GaSb superlattices, quantum cascade lasers, multi-quantum wells, distributed Bragg reflectors, and vertical cavity surface emitting lasers) using the high resolution X-ray diffraction technique.

Ewa Bobko received the Ph.D. degree in the field of natural sciences in the discipline of physical science in 2021, from the University of Rzeszow, Poland. Her research activity focuses on structural characterization of semiconductors and fabrication of nanostructures by lithographic methods.

Eugeniusz Szeregij has over 30 years of academic and industry experience in the semiconductors physics and technology and development of the material control applications using the IR-diagnostic. He is passionate about adoption of the micro-Raman method for material control through scientific communication. He received his PhD in A.F. Joffe Physics-Technical Institute in Leningrad (USSR) (now St. Petersburg, Russia). From 1992 to 2019 he was Full Professor at the University of Rzeszow where he created on the basis of European funds the Centre for Microelectronics and Nanotechnology with Laboratories of MBE-technology, photolithography and IR as well Raman control of produced nanostructures.

Jakub Grendysa received the M.Sc. degree in Physics from the University of Rzeszow, Poland, in 2009. He is currently an MBE Technology Specialist at the Center for Microelectronics and Nanotechnology, University of Rzeszow, and the International Centre for Interfacing Magnetism and Superconductivity with Topological Matter – MagTop of Institute of Physics, Polish Academy of Sciences (IF PAN). His research activity focuses on the production of II–VI structures by molecular beam epitaxy, in particular for mercury compounds.

Grzegorz Tomaka received the Ph.D. degree from the University of Rzeszow in 2008. He is the author of many papers on electron transport in two-dimensional structures based on AIIBVI and AIIIBV materials. He performs experiments at low temperatures (from 200 mK) and magnetic fields up to 14 T. He is interested in 3D topological Dirac semimetal (massless Dirac fermions) based on HgCdTe. He examines topological insulators based on strained semi-metallic HgCdTe layers (MBE growth), where he observed high-temperature stability of electron transport in semiconductors with strong spin-orbital interaction. He obtained magnetophonon resonance on the phonon frequency difference in quasi-free-standing graphene.

Dariusz Żak received the Ph.D. degree in Electronic Engineering from Rzeszow University of Technology, Poland. He is currently an employee of the University of Rzeszow. His main research activity focuses on cryogenic experiments, AFM, Raman and FTIR techniques, MMM, and UT diagnostics.

Dariusz Płoch received the Ph.D. degree in solid state physics from the University of Rzeszow, Poland, in 2012. He is currently Assistant Professor in the Center for Microelectronics and Nanotechnology, University of Rzeszow. He has coauthored 25 scientific publications. His research activity focuses on the use of electron beam lithography (EBL) in semiconductors and the scanning electron microscopy (SEM) and scanning probes microscopy (SPM) in nanotechnology.

Agata Jasik received the Ph.D. degree in Technical Science from Warsaw University of Technology, Warsaw, Poland, in 2002. From 1995 to 2006 she worked at the Institute of Electronic Materials Technology. Her research included the metaloorganic vapor phase epitaxy of semiconductor structures and its characterization. Since 2006 she has worked at the Łukasiewicz Research Network – Institute of Microelectronics and Photonics and her main field activity is the molecular beam epitaxy of III-V optoelectronic devices such as lasers, modulators and infrared detectors. In particular, focal plane arrays from the IR range are in the focus of her actual interests.